Eur. Phys. J. A **8**, 197–204 (2000)

THE EUROPEAN PHYSICAL JOURNAL A

Neutrons produced by 1.22 GeV antiproton interactions with nuclei

T. von Egidy[1], P. Figuera[2,a], J. Galin[3], F. Goldenbaum[2,b], Ye.S. Golubeva[4], M. Hasinoff[1,5], D. Hilscher[2], A.S. Iljinov[4], U. Jahnke[2], M. Krause[1], W. Kurcewicz[6], X. Ledoux[3,c], B. Lott[3], L. Maier[1], M. Manrique de Lara[1], G. Pausch[7], L. Pienkowski[8], B. Quednau[3], W. Schott[1], W.U. Schröder[9], and J. Tõke[9]

[1] Physik-Department, Technische Universität München, D-85748 Garching, Germany
[2] Hahn-Meitner-Institut Berlin, D-14109 Berlin, Germany
[3] GANIL, IN2P3/CNRS-DSM/CEA, F-14076 Caen, France
[4] Institute for Nuclear Research, Russian Academy of Sciences, 117312 Moscow, Russia
[5] University of British Columbia, Vancouver, B.C., Canada V6T 1Z1
[6] Institute of Experimental Physics, Warsaw University, PL-00-681 Warszawa, Poland
[7] Forschungszentrum Rossendorf, D-01314 Dresden, Germany
[8] Heavy Ion Laboratory, Warsaw University, Pl-02-097 Warszawa, Poland
[9] University of Rochester, NY 14627, USA

Received: 25 February 2000 / Revised version: 15 May 2000
Communicated by D. Schwalm

Abstract. Inclusive neutron energy spectra were measured by time of flight using 1.22 GeV antiprotons from LEAR, CERN, as projectiles and targets from natural Al, Cu, Ag, Ho, Ta, Au, Pb, Bi, U. The sum of two Maxwellian distributions was fitted to the spectra $\mathrm{d}^2\sigma/(\mathrm{d}\Omega\mathrm{d}E)$ obtained at several forward and backward angles yielding neutron multiplicities M_i and slope or temperature parameters T_i for the low-energy (evaporative, $i = 1$) and high-energy (pre-equilibrium, $i = 2$) parts, respectively. M_1 increases with A, proportional to the nuclear volume, and M_2 is growing with $A^{1/3}$, proportional to the nuclear radius. The T parameters are nearly independent of A. The results are compared with previous multiplicity measurements with a 4π neutron detector, intranuclear cascade calculations and neutron spectra from stopped antiproton annihilation on nuclei. With the measured proton spectra also the ratio of emitted neutrons to protons was determined for Au.

PACS. 25.43.+t Antiproton-induced reactions – 24.60.Dr Statistical compound nucleus reactions – 24.75.+i General properties of fission

1 Introduction

Antiprotons ($\overline{\mathrm{p}}$) are a very interesting tool to produce very hot nuclei up to thermal excitation energies of 1 GeV. In contrast to heavy-ion reactions these excited nuclei are produced without compression and without high angular momentum. Consequently, different and new processes are expected. Many experiments were performed at the Low Energy Antiproton Ring LEAR at CERN, Geneva, to investigate the heating of nuclei using *stopped antiprotons* [1–11]. Antiprotons at rest form antiprotonic atoms, cascade down to lower orbits and annihilate with one nucleon at the nuclear surface. The annihilation produces between two and eight pions, sometimes *via* intermediate mesons, which have energies up to several hundred MeV.

Some pions penetrate the nucleus and start an intranuclear cascade with the emission of fast neutrons, protons and other light charged particles. A very broad distribution of hot nuclei is obtained which cool down mainly by evaporation of neutrons and light charged particles. In heavier nuclei also fission takes place [8,10,11]. The spectra of emitted particles have been carefully measured [3, 5,9]. All these experimental results can be quite well reproduced by intranuclear cascade (INC) and evaporation calculations using Monte Carlo methods [12,13].

The initial step of the interaction of *fast antiprotons* with nuclei is quite different. The fast antiproton sees the nucleus nearly as a black sphere [14] and annihilates with a nucleon slightly deeper within the nuclear surface. The annihilation pions are kinematically focused towards the nucleus. Hence, more and faster pions heat the nucleus more than after the annihilation of stopped antiprotons.

[a] *Present address:* INFN-Laboratorio Nazionale del Sud, I-95123 Catania, Italy
[b] *Present address:* Forschungszentrum Jülich, Institut für Kernphysik, D-52428 Jülich, Germany
[c] *Present address:* DPTA/SPN, Commissariat à l'Energie Atomique, F-91680 Bruyères-le-Châtel, France

Table 1. Used targets and their thicknesses.

Target	Thickness (g/cm^2)	Target	Thickness (g/cm^2)
^{27}Al	0.35	^{197}Au	1.9
^{nat}Cu	1.8	^{nat}Pb	2.27
^{nat}Ag	1.06	^{209}Bi	1.9
^{165}Ho	0.53	^{238}U	5.72
^{181}Ta	3.32	—	—

It is expected that the heating is "smooth" and faster compared to heavy-ion reactions.

In order to study these processes in detail a new detector was constructed which measures in 4π geometry the multiplicities of the emitted neutrons (Berlin Neutron Ball = BNB) and charged particles and fragments (Berlin Silicon Ball = BSiB) [15,16]. Some exciting results obtained with this new detector have already been published [14,17–21]. For instance, an average number of only 1.0 intermediate-mass fragments was found for the most highly excited heavy nuclei [19] indicating that multifragmentation does not play as significant a role as in many high-energy heavy-ion reactions. Neutron multiplicities of up to 50 corresponding to thermal excitation energies up to 1 GeV were observed in Au, Bi and U targets. Unfortunately, this detector does not determine the energy spectra of the neutrons. However, these neutron spectra contain important information on the reaction, heating and cooling mechanisms, on temperatures and on the energy balance. Furthermore they are helpful to check the efficiency correction of the BNB. Therefore, a specific experiment was carried out to measure the neutron energy spectra after annihilation of fast antiprotons in a series of targets. A similar setup was used for the experiments with stopped antiprotons [5,9].

2 Experiment

The experiments were performed at the Low Energy Antiproton Ring LEAR at CERN, Geneva (PS208). Antiprotons with kinetic energy $E_{\overline{p}} = 1.22$ GeV annihilated within a wide range of targets (Al-U, see table 1). By using targets with rather small thicknesses mainly annihilation in flight was observed without secondary reactions. The resulting inclusive neutron spectra were measured with the time-of-flight method (TOF).

The incoming antiproton beam passed several scintillation detectors, the target and two scintillators behind the target. The 2 mm thick first plastic scintillator placed 16.14 m upstream from the target was used as a start detector for the TOF measurement. It was positioned in an air gap between the LEAR and the experimental vacuum system. During a beam spill (ca. 1 h) antiprotons hit this scintillator at a rate of about $10^5\,s^{-1}$. The antiprotons then traveled inside a 15 cm diameter vacuum tube with a wall thickness of 2 mm steel and passed plastic scintillator diaphragms, which were operated as veto counters to control the adjustment of the beam. The antiprotons hit the

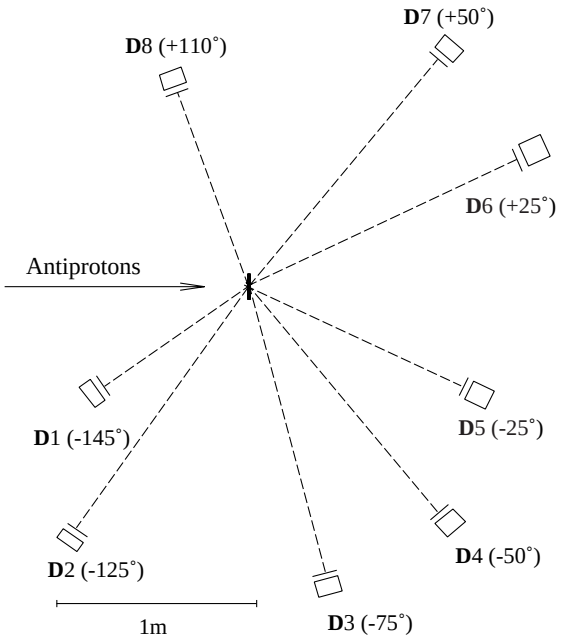

Fig. 1. Neutron detector setup at the antiproton beam. The angles of the detectors (D1-D8) towards the $\overline{p}$ beam are $-145°$, $-125°$, $-75°$, $-50°$, $-25°$, $+25°$, $+50°$, $+110°$, respectively. In front of each liquid scintillator a 3 mm thick plastic scintillator is mounted to identify charged particles.

5 cm × 5 cm quadratical target which absorbs only a small fraction of the antiproton beam. The antiprotons without interaction in the target left the vacuum tube 4.37 m behind the target through a 1 mm thick steel window and passed additional plastic scintillators used as veto counters for beam alignment.

The neutron TOF spectra were measured with eight NE213 liquid scintillation counters (D1-D8) with diameters and thicknesses in the ranges 10.2–12.7 cm and 5.1–10.2 cm, respectively (cf. fig. 1). A 3 mm thick plastic scintillator was mounted in front of each liquid scintillator and used as a charged-particle veto counter. The detectors were positioned around the target at angles between $-145°$ and $+110°$ and distances between 0.9 m and 1.5 m. The liquid scintillation counters provided also the stop signals for the TOF measurement. Neutron counters similar to the used ones are described in detail in ref. [9].

In order to distinguish between neutrons and γ-rays in the scintillation counters, a pulse shape parameter $\Delta E = E_1 - E_2$ was derived from each scintillator detector in addition to the signal $E_0 = E_1 + E_2$. E_1 denotes the integrated intensity of the rising part of the liquid scintillator signal up to the maximum and E_2 the integrated intensity of the falling part after the maximum. For particle identification two-dimensional plots of the energy difference ΔE *vs.* total deposited recoil energy E_0 yielded separated groups of neutrons and γ-ray events (cf. fig. 2).

An additional selection of neutron events was made in the E_0 *vs.* E plane, where E denotes the neutron kinetic energy deduced from TOF exploiting relativis-

Table 2. Fitted evaporation and pre-equilibrium parameters K and T of the neutron production cross-section $\mathrm{d}^2\sigma/(\mathrm{d}\Omega\mathrm{d}E)$. The errors of K_1, K_2, T_1 amount to ±10%, while the error of T_2 is about ±5%. For Al and Cu, however, the error of T_1 is ±30% and ±15%, respectively.

	K_1 (mb/sr)					K_2 (mb/sr)				
	−145 °	−125 °	−75 °	−50 °	+50 °	−145 °	−125 °	−75 °	−50 °	+50 °
Al	62	73	90	96	111	94	119	172	236	238
Cu	327	360	379	431	400	270	337	449	596	557
Ag	823	912	972	931	1000	466	569	750	935	909
Ho	1960	2200	2330	2410	2370	803	1000	1290	1630	1500
Ta	2380	2630	2720	2800	2700	854	1100	1310	1600	1570
Au	2660	2930	3120	3090	2900	942	1190	1500	1800	1650
Pb	2690	2970	3080	3190	3140	928	1150	1410	1730	1660
Bi	2890	3200	3260	3290	3170	1010	1240	1550	1820	1750
U	3890	4290	4050	4110	4410	1080	1340	1600	1910	1890

	T_1 (MeV)					T_2 (MeV)				
	−145 °	−125 °	−75 °	−50 °	+50 °	−145 °	−125 °	−75 °	−50 °	+50 °
Al	3.9	3.1	3.5	4.6	3.9	41.8	36.2	47.6	59.2	55.1
Cu	4.2	3.6	3.9	4.3	4.1	39.6	36.6	46.8	54.0	52.1
Ag	4.0	3.6	3.8	4.0	4.0	38.7	33.1	42.6	47.9	50.0
Ho	3.8	3.6	3.7	3.8	3.8	34.4	32.6	40.7	45.7	45.2
Ta	4.1	3.7	3.9	4.1	4.1	34.7	32.2	38.2	42.7	45.0
Au	3.9	3.6	3.8	4.1	4.0	35.4	31.6	39.4	43.6	43.2
Pb	4.0	3.7	3.9	4.2	3.9	34.5	32.3	39.6	44.4	43.1
Bi	4.0	3.7	3.9	4.2	4.0	35.6	32.2	39.5	43.3	43.3
U	3.6	3.3	3.5	3.7	3.5	34.0	32.0	38.1	40.6	40.2

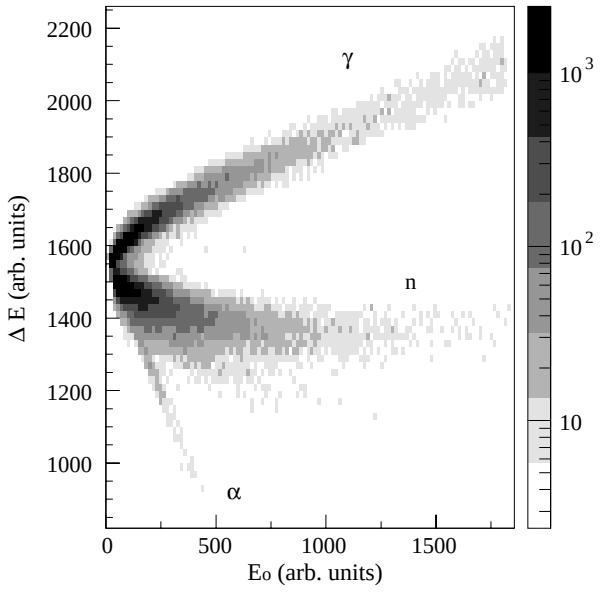

Fig. 2. Energy difference ΔE *vs.* total recoil energy E_0 (detector pulse height), both measured with the liquid scintillator detector D3 using a 1.9 g/cm^2 thick Bi target. Gamma rays and neutrons are clearly distinguished. The α particles are produced within the scintillator by neutrons with the ^{12}C (n,α) ^{9}Be reaction.

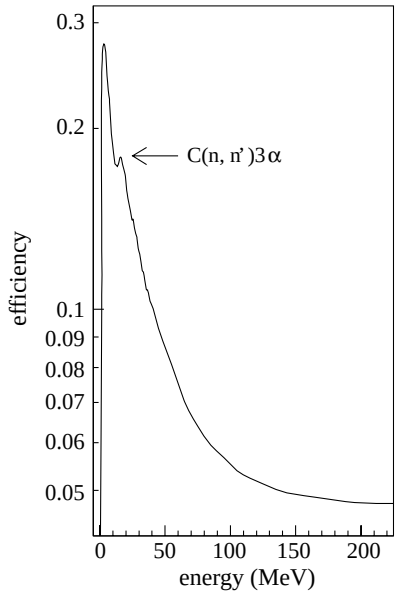

Fig. 3. Intrinsic neutron detection efficiency ϵ *vs.* neutron energy E for detector D1 as calculated by means of the MC program CECIL [22] for a NE213 detector with diameter and thickness of 12.6 and 5.08 cm, respectively. The detection threshold was $E = 1.23$ MeV as determined with a ^{22}Na source and measured TOF spectrum. The peak in the efficiency near 20 MeV comes from the ^{12}C (n,n′)3α reaction.

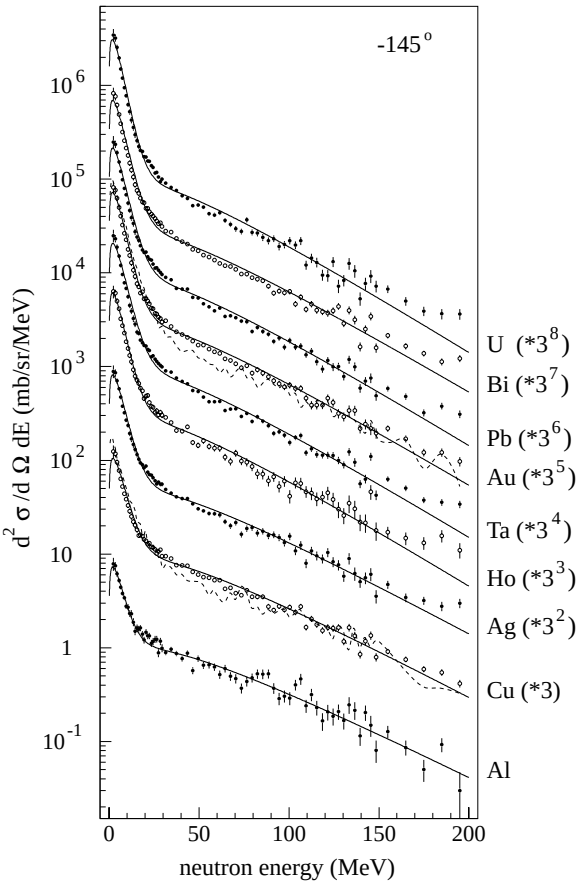

Fig. 4. Double differential inclusive neutron production cross-sections $\mathrm{d}^2\sigma/(\mathrm{d}\Omega\mathrm{d}E)$ *vs.* E for Al, Cu, Ag, Ho, Ta, Au, Pb, Bi, and U targets at an emission angle of $-145°$. The dots denote the measured points, the drawn lines the function of eq. (1) fitted to the measured points with K_i and T_i $(i = 1, 2)$ as fit parameters and the dashed lines INC calculations, respectively. The cross-sections have been multiplied by 3^n as indicated.

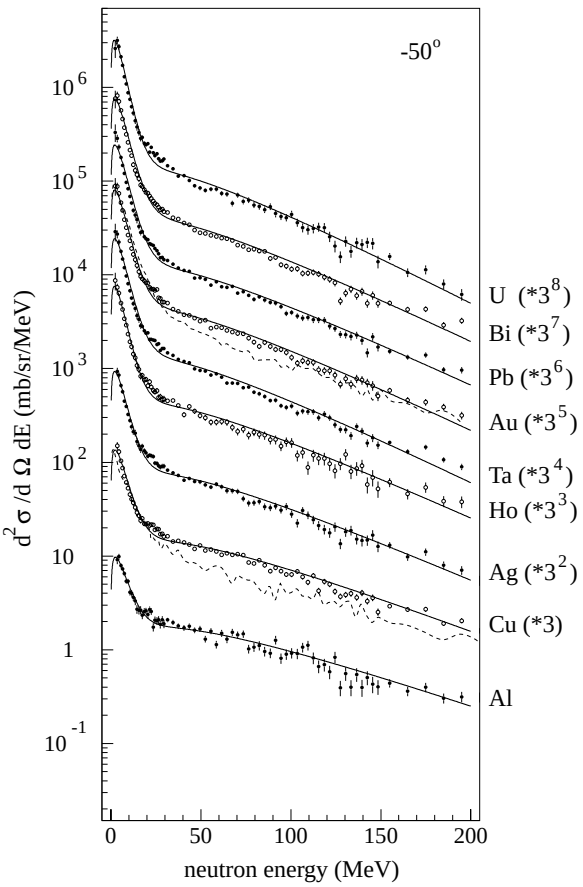

Fig. 5. $\mathrm{d}^2\sigma/(\mathrm{d}\Omega\mathrm{d}E)$ *vs.* E at an emission angle of $-50°$; else as fig. 4.

tic kinematics. Signals from neutrons, which were scattered in the surrounding material before reaching the detectors, were partly rejected by imposing the condition $E_0 \leq E$. Figure 3 shows the intrinsic neutron detection efficiency $\epsilon(E)$ of D1, calculated with the program by Cecil *et al.* [22] for a detection threshold at 1.23 MeV. By means of the measured neutron spectra and $\epsilon(E)$ the double-differential neutron production cross-section $\mathrm{d}^2\sigma/(\mathrm{d}\Omega\mathrm{d}E)$ after 1.22 GeV $\overline{\mathrm{p}}$ annihilation is obtained. The threshold for neutron detection was between 1.0 and 2.0 MeV. Consequently the spectra below about 2 and 4 MeV are not reliable resulting in considerable uncertainties for the determination of evaporative neutron multiplicities.

3 Results

Experimental double-differential neutron cross-sections $\mathrm{d}^2\sigma/(\mathrm{d}\Omega\mathrm{d}E)$ measured for nine targets are displayed in figs. 4 and 5 at a backward angle of $-145°$ and a forward angle of $-50°$ as examples. These distributions are seen to consist essentially of two parts, one low-energy component (< 20 MeV) originating from the neutron evaporation and one fast-neutron component (> 20 MeV) extending to high energies due to neutron emission during the fast intranuclear cascade. Although there is no physical justification to fit the INC component with a Maxwellian distribution, such a distribution has nevertheless been used as a functional dependence, with thus T_2 being not a temperature. Consequently, $\mathrm{d}^2\sigma/(\mathrm{d}\Omega\mathrm{d}E)$ can be approximated by the sum of two Maxwellian distributions [23],

$$\frac{\mathrm{d}^2\sigma}{\mathrm{d}\Omega\mathrm{d}E} = K_1 \frac{\sqrt{E}}{T_1^{3/2}}\, e^{-E/T_1} + K_2 \frac{\sqrt{E}}{T_2^{3/2}}\, e^{-E/T_2}. \qquad (1)$$

T_i $(i = 1, 2)$ are spectral shape parameters with T_1 connected to the temperature of the evaporating system. K_i are related to $\mathrm{d}\sigma/\mathrm{d}\Omega$ by $\mathrm{d}\sigma/\mathrm{d}\Omega = (\sqrt{\pi}/2)(K_1(\theta)+K_2(\theta))$. The spectra were fitted with eq. (1) above 2–4 MeV. The resulting fit parameters K_i and T_i are listed in table 2. The given errors of the K and T values include statistical and systematic errors. The systematic errors were estimated from deficiencies of the fit procedure (*e.g.*, only two exponentials) and possible electronic cuts during the measurement by looking at the variations of the fit procedure or the changing thresholds. The limited time resolution was also taken into account in the errors. The errors of the

T_1 values (±10%) are about twice as large as for T_2. In particular for the light targets Al and Cu the error of T_1 was ±30% and ±15%, respectively. The spectra measured at +110° (D8) and ±25° (D5, D6) were not included in table 2. For detector D8 the pulse shape discrimination was not good enough for reliable data analysis while the detectors D5 and D6 are contaminated with too much background from annihilation of scattered antiprotons in the beam tube close to the ±25° detectors. For the other detectors the background was sufficiently small to be neglected.

Since the velocity of the emitting source is relatively small [24] as compared to the neutron velocity, it was neglected in the given formula (1). The fitted curves obtained with this function are also shown in figs. 4 and 5. In spite of the good overall agreement between the measured and fitted spectra the experimental yield is underrepresented by the fit near 25 MeV in most cases. This indicates that for a better reproduction of the experimental results a third Maxwellian distribution would be necessary representing the intermediate pre-equilibrium neutron emission. This third component was used by Polster *et al.* [5,9] for the fit of neutron spectra after annihilation of stopped antiprotons in heavier targets. However, since an increased number of free fit parameters would have made the fit less stable we preferred therefore a fit with only two Maxwellian distributions which also facilitates the comparison of the different targets.

The evaporation neutrons are supposed to have isotropic angular distributions. Consequently, average values of K_1 and T_1 of the five measured angles (−145°, −125°, −75°, −50°, +50°) are given for each target in table 3. The weak angular dependence of K_1 (due to the antiproton momentum) was neglected. The fast-neutron components, instead, have higher intensities and slightly higher T-values in beam direction (small angles). Since it is difficult to assume a meaningful angular distribution, also the average values $\overline{T}_2$ are listed in table 3. The angular distribution of K_2 was assumed to be described by

$$K_2(\theta) = C \exp(a \cos\theta). \tag{2}$$

Figure 6 shows the angular distributions of K_2 for the Cu, Ho and U targets together with the fitted functions (2). Parameters C and a were determined for each target with a least squares fit. The a-values are decreasing with A from 0.58 for Al to 0.37 for Ta and 0.33 for U. The average K_2 values are obtained by integration over the full solid angle:

$$\begin{aligned}\overline{K}_2 &= \frac{C}{2}\int_{-1}^{+1} \exp(a\cos\theta)\,\mathrm{d}(\cos\theta) \\ &= \frac{C}{2a}(\exp(a) - \exp(-a)).\end{aligned} \tag{3}$$

The average neutron multiplicities $\overline{M}_i$ are calculated from $\overline{K}_i$ with

$$\overline{M}_i = \frac{2\pi^{3/2}}{\sigma_{\mathrm{inel}}}\overline{K}_i, \tag{4}$$

where σ_{inel} is the total inelastic reaction cross-section which is essentially given by the annihilation cross-section.

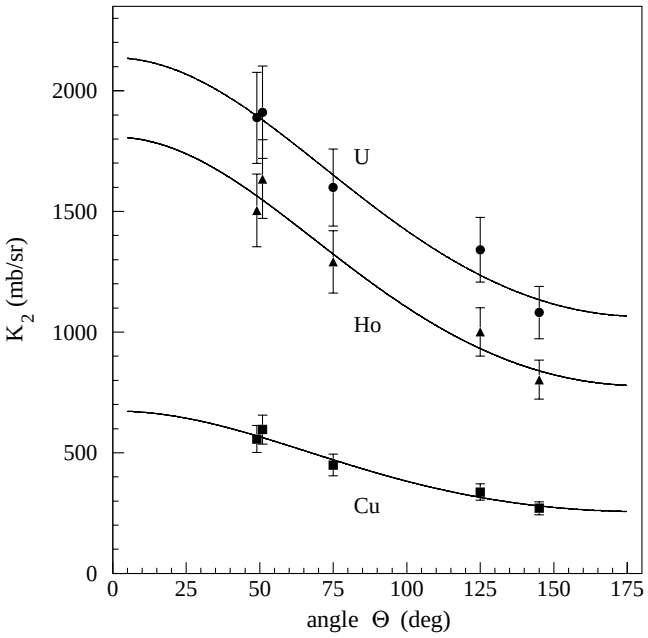

Fig. 6. Angular distribution of the fast neutrons after $\overline{\mathrm{p}}$ annihilation in Cu, Ho and U targets (K_2).

The used σ_{inel} values were calculated with the experimentally derived formula [14,17]:

$$\sigma_{\mathrm{inel}} = \left(1.38A^{1/3}\right)^2\pi. \tag{5}$$

The values $\overline{K}_2$, $\overline{M}_2$ and σ_{inel} are also listed in table 3. The target mass dependence of all $\overline{T}_i$ and $\overline{M}_i$ values is displayed in fig. 7. The experimental values were fitted with ad-hoc functions, that is $\overline{M}_1 = 0.084 \cdot (A - 8.9)$, $\overline{M}_2 = 1.23 \cdot (A - 14.9)^{1/3}$, $\overline{T}_1 = 3.84\,\mathrm{MeV}$ and $\overline{T}_2 = (21.7 + 7970/(A + 274))\,\mathrm{MeV}$.

4 Discussion

Inspection of table 3 and fig. 7 reveals several striking features. For all targets the apparent evaporation temperature $\overline{T}_1$ remains essentially constant with an average value of $3.84 \pm 0.20\,\mathrm{MeV}$. The temperature $\overline{T}_1$, however, is the average over the whole neutron cascade while the initial temperature is about $(12/11) \cdot \overline{T}_1$ [25]. In terms of the Fermi gas model, this translates into an average initial excitation energy E^* of the target-like nucleus after the prompt intranuclear cascade of $E^* = a \cdot (\overline{T}_1 \cdot 12/11)^2$. Assuming a level density parameter $a = A/10\,\mathrm{MeV}^{-1}$ we obtain $E^*/A = 1.9 \pm 0.6$, 1.8 ± 0.3, and $1.5 \pm 0.3\,\mathrm{MeV/nucleon}$ from table 3 for Cu, Au, and U, respectively. This result agrees within the errors with the respective average excitation energies of 2.53 ± 0.25, 1.65 ± 0.17 and $1.52 \pm 0.15\,\mathrm{MeV/nucleon}$ as deduced by Goldenbaum *et al.* [17] by employing the caloric method, *i.e.* by summing up the energy removed by all evaporated neutrons and light charged particles.

The multiplicities of evaporated neutrons $\overline{M}_1$ increase nearly linearly with A. This indicates an increase of the

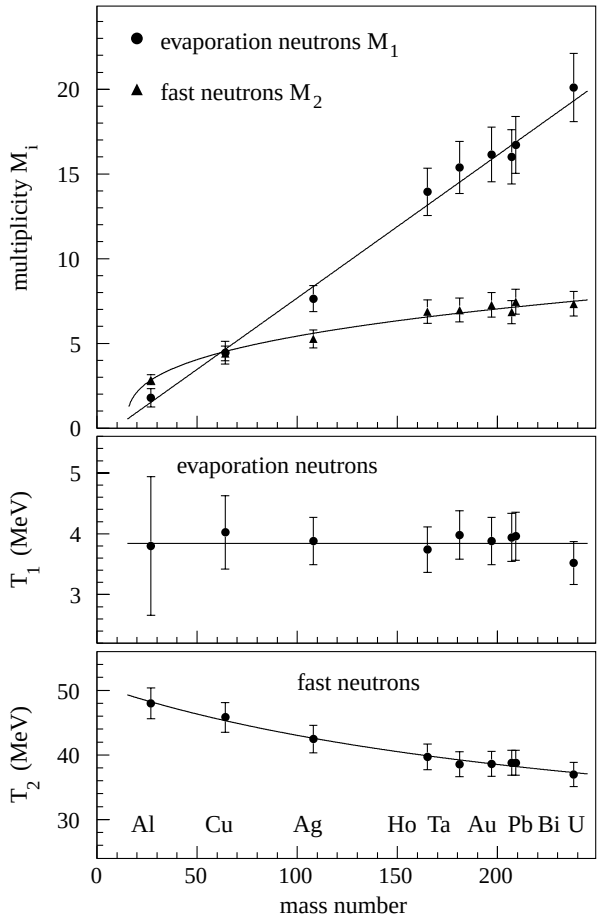

Fig. 7. Target mass dependence of the neutron multiplicities $\overline{M}_i$ and the $\overline{T}_i$ parameters. Note the supressed zero in the ordinate of the lower two panels.

deposited excitation energy with A. The slope parameters $\overline{T}_2$ of the fast neutron spectra are decreasing from Al to Ag and then remain rather constant near 39 MeV for heavier targets. This means that the process of fast neutron emission is rather independent of A for $A > 100$. The multiplicity of fast neutrons seems to increase with $A^{1/3}$ being proportional to the nuclear radius. This behavior indicates that the path length of the pions or fast nucleons in the nucleus is responsible for the number of emitted neutrons.

It is very interesting to compare the values of T_i and M_i with the corresponding results obtained by Polster *et al.* [9] with stopped antiprotons, because it demonstrates the influence of the increased antiproton energy and of the larger number and energy of pions interacting with the nucleus. The total neutron multiplicities for the different targets are compared in table 4. The neutron multiplicities for all targets are about 60% larger at 1.22 GeV than for stopped antiprotons. In heavier targets about 9 additional neutrons are emitted by fast antiprotons. However, a detailed comparison sheds more light on the similarities and differences. For evaporation neutrons the multiplicities (M_1) are about 20–50% larger for fast than for stopped antiprotons and the T_1 parameter is about 1–1.5 MeV larger for fast antiprotons and heavy nuclei. However, this latter finding is partially due to the fact that for heavy nuclei a three component fit was employed in ref. [9] which tends to reduce the temperature of the evaporative component. For fast neutrons from the INC the T parameters are very similar for stopped and fast antiprotons while the multiplicities increase in most cases from about 2.5 to about 7 for fast antiprotons. It is surprising that the higher energy of the annihilation pions does not cause higher fast neutron energies but more collisions in the INC and thus larger multiplicities of fast neutrons.

In the cases of Cu and Au in addition to the measured and fitted spectra shown in figs. 4 and 5 also spectra calculated with the INC model (and filtered with the experimental detector efficiency) are displayed. The used INC model is discussed in refs. [8,10,12,14]. While the agreement for the evaporative part is satisfactory, the calculated fast neutron spectra are too low, especially at $-50°$. The reason for this discrepancy is not evident.

One of the purposes of the present investigation is the comparison with the total neutron multiplicities obtained with the Berlin Neutron Ball [24]. This detector measures the neutron multiplicity in each reaction but does not yield any information on the energy of the emitted neutrons. In order to correct for the neutron energy dependent efficiency of this detector (typically about 82% and 21% for M_1 and M_2, respectively [26]) the neutron energy distribution must be known. From the present investigation we have obtained the effective efficiency $\epsilon^{\rm eff}_{\rm BNB}$ by folding the energy dependent efficiency of BNB with the measured spectral shape by using the mean parameters given in table 3. The result for $\epsilon^{\rm eff}_{\rm BNB}$ is given in table 4 which was then used to correct the neutron multiplicity $M_{\rm BNB}$ as measured with BNB. These values [24] are also given in table 4. It is satisfying to see that the BNB multiplicities are very similar to those measured in the present experiment. This agreement furthermore confirms that the procedure to employ the Maxwellian distribution to extrapolate the measured neutron energy spectra below 2–4 MeV is correct, since the BNB essentially has no low energy cut off energy.

In refs. [17–21] the thermal excitation energy of each induced reaction was reconstructed by exploiting the measured associated multiplicity of neutrons and light charged particles. This procedure requires that the particles have been evaporated from an equilibrated source. The measured neutron multiplicity consists, however, of the sum of evaporated and pre-equilibrium neutrons detected with high and low efficiency, respectively. Following model calculations it was assumed in the above references that the measured neutron multiplicity can be identified with the multiplicity of evaporated neutrons. In table 3 the measured (not corrected for efficiency) mean neutron multiplicity $M_{\rm BNB}$ is given in the last column. By comparing these numbers with the $\overline{M}_1$-values we observe that indeed $M_{\rm BNB} \approx \overline{M}_1$ confirming the assumptions made in refs. [17–21]. This observation is due to an accidental compensation of the somewhat smaller than 1 efficiency for

Table 3. Average K, T and M values deduced from the fitted neutron spectra. $\sigma_{\rm inel}$ was calculated with $(1.38 \cdot A^{1/3})^2 \cdot \pi$ [14, 17]. The errors of K_1, K_2, T_1 amount to $\pm 10\%$, while the error of T_2 is about $\pm 5\%$. For Al and Cu, however, the error of T_1 is $\pm 30\%$ and $\pm 15\%$, respectively. In the last column the mean neutron multiplicity $M_{\rm BNB}$ as measured with BNB is given as well [24] with the errors in parentheses.

Target	$\sigma_{\rm inel}$ (mb)	$\overline{K}_1$ (mb/sr)	$\overline{M}_1$	$\overline{T}_1$ (MeV)	$\overline{K}_2$	$\overline{M}_2$	$\overline{T}_2$ (MeV)	$M_{\rm BNB}$
^{27}Al	538	86	1.8	3.8	140	2.9	48.0	2.6(3)
$^{\rm nat}$Cu	950	379	4.5	4.0	380	4.4	45.8	5.0(6)
$^{\rm nat}$Ag	1353	928	7.6	3.9	640	5.3	42.5	8.0(10)
^{165}Ho	1800	2250	14.0	3.7	1110	6.9	39.7	12.8(15)
^{181}Ta	1914	2640	15.4	4.0	1200	7.0	38.6	14.7(18)
^{197}Au	2026	2940	16.2	3.9	1320	7.3	38.6	15.4(19)
$^{\rm nat}$Pb	2095	3010	16.0	3.9	1290	6.9	38.8	16.3(20)
^{209}Bi	2107	3160	16.7	4.0	1410	7.5	38.8	—
^{238}U	2298	4150	20.1	3.5	1510	7.3	37.0	18.2(22)

Table 4. Comparison of the total neutron multiplicities from the present measurement ($\overline{M}_1 + \overline{M}_2$) and from a measurement with the 4π neutron detector BNB [24] ($M^{\rm corr}_{\rm BNB}$) which was corrected for the BNB detection efficiency $\epsilon^{\rm eff}_{\rm BNB}$; The total neutron multiplicities $\overline{M}_{\rm stopped\overline{p}} = \overline{M}_1 + \overline{M}_2(+\overline{M}_3)$ after annihilation of stopped antiprotons [9] are also given. The errors of $M^{\rm corr}_{\rm BNB}$ and $\overline{M}_{\rm stopped\overline{p}}$ are given in parentheses.

Target	$\overline{M}_1 + \overline{M}_2$	$M^{\rm corr}_{\rm BNB}$	$\epsilon^{\rm eff}_{\rm BNB}$	$\overline{M}_{\rm stopped\overline{p}}$
^{27}Al	4.65	5.1(6)	0.51	3.08(31)
$^{\rm nat}$Cu	8.86	8.8(10)	0.57	5.9(4)
$^{\rm nat}$Ag	12.9	13.1(16)	0.61	8.0(7)
^{165}Ho	20.8	19.6(25)	0.65	12.2(9)
^{181}Ta	22.4	22.2(27)	0.66	14.0(11)
^{197}Au	23.4	23.2(28)	0.66	14.9(9)
$^{\rm nat}$Pb	22.9	24.4(29)	0.67	—
^{209}Bi	24.2	—	0.66	15.6(11)
^{238}U	27.5	26.5(31)	0.69	18.1(14)

evaporative neutrons by the detection of energetic neutrons.

5 Ratio of energetic neutrons to energetic protons

Though the main emphasis of the present experiment was the measurement of neutron spectra, we have obtained also information on the energetic proton spectra by requiring coincidences with the scintillator paddle in front of each neutron detector. This method has been explained in detail in ref. [9]. The unexpected finding for stopped antiprotons was that the neutron to proton ratio is almost twice as large as the N/Z ratio of the target [9]. For fast antiprotons we have found, however, that for the Au target the n/p ratio amounts to 1.50 ± 0.25 at nucleon energies of about 100 ± 25 MeV. This finding for fast antiprotons is within the errors in agreement with the N/Z ratio of Au (1.49) and the predictions of INC calculations (n/p=1.5).

6 Summary

The spectra of neutrons emitted after annihilation of 1.22 GeV antiprotons at various target nuclei yielded a wealth of new information on very hot nuclei. In particular the observation of a strong evaporative component in the spectra of emitted neutrons can be taken as an additional important confirmation of the thermalization hypothesis made in previous studies of the decay properties of antiprotonic heated nuclei. The spectra were fitted with two Maxwellian distributions for fast and evaporation neutrons. The resulting multiplicities and slope parameters show specific dependencies on the target mass number A and are compared with INC calculations and corresponding values of stopped-antiproton annihilation. The agreement with the INC model is good. The higher available energy of 1.22 GeV for the $\overline{\rm p}$ annihilation increases the multiplicities of fast INC neutrons and the temperature of the evaporation neutrons. The measured integral neutron multiplicities are in excellent agreement with a previous measurement employing a 4π neutron detector.

The excellent antiproton beam of LEAR and the help of the LEAR team is very much appreciated. We wish to thank F.J. Hartmann and B. Ketzer for discussions. The work was supported by the Beschleunigerlaboratorium der Universität und Technischen Universität München.

References

1. T. von Egidy, Nature **328**, 773 (1987).
2. E.F. Moser, H. Daniel, T. von Egidy, F.J. Hartmann, W. Kanert, G. Schmidt, Ye.S. Golubeva, A.S. Iljinov, M. Nicholas, J.J. Reidy, Z. Phys. A **333**, 89 (1989).

3. P. Hofmann, F.J. Hartmann, H. Daniel, T. von Egidy, W. Kanert, W. Markiel, H.S. Plendl, H. Machner, G. Riepe, D. Protic, K. Ziock, R. Marshall, J.J. Reidy, Nucl. Phys. A **512**, 669 (1990).
4. T. von Egidy, H.H. Schmidt, Z. Phys. A **341**, 79 (1991).
5. D. Polster, D. Hilscher, H. Rossner, W. Schmid, P. Baumann, H. Daniel, T. von Egidy, F.J. Hartmann, P. Hofmann, Y.S. Kim, M.S. Lotfranaei, Phys. Lett. B **300**, 317 (1993).
6. J. Jastrzebski, W. Kurcewicz, P. Lubinski, A. Grabowska, A. Stolarz, H. Daniel, T. von Egidy, F.J. Hartmann, P. Hofmann, Y.S. Kim, A.S. Botvina, Ye.S. Golubeva, A.S. Iljinov, G. Riepe, H.S. Plendl, Phys. Rev. C **47**, 216 (1993).
7. T. von Egidy, Acta Phys. Pol. B **24**, 1823 (1993).
8. P. Hofmann, A.S. Iljinov, Y.S. Kim, M.V. Mebel, H. Daniel, P. David, T. von Egidy, T. Haninger, F.J. Hartmann, J. Jastrzebski, W. Kurcewicz, J. Lieb, H. Machner, H.S. Plendl, G. Riepe, B. Wright, K. Ziock, Phys. Rev. C **49**, 2555 (1994).
9. D. Polster, D. Hilscher, H. Rossner, T. von Egidy, F.J. Hartmann, J. Hofmann, W. Schmid, I.A. Pshenichnov, A.S Iljinov, Y.S. Golubeva, H. Machner, H.S. Plendl, A. Grochulska, J. Jastrzebski, W. Kurcewicz, P. Lubinsky, J. Eades, S. Neumaier, Phys. Rev. C **51**, 1167 (1995).
10. Y.S. Kim, A.S. Iljinov, M.V. Mebel, P. Hofmann, H. Daniel, T. von Egidy, T. Haninger, F.J. Hartmann, H. Machner, H.S. Plendl, G. Riepe, Phys. Rev. C **54**, 2469 (1996).
11. W. Schmid, T. von Egidy, F.J. Hartmann, J. Hoffmann, S. Schmid, D. Hilscher, D. Polster, H. Rossner, A.S. Iljinov, M.V. Mebel, D.I. Ivanov, V.G. Nedorezov, A.S. Sudov, H. Machner, H.S. Plendl, J. Eades, S. Neumaier, Phys. Rev. C **55**, 2965 (1997).
12. A.S. Iljinov, V.I. Nazaruk, S.E. Chigrinov, Nucl. Phys. A **382**, 378 (1982).
13. J. Cugnon, J. Vandermeulen, Nucl. Phys. A **445**, 717 (1985).
14. S. Schmid, W. Schmid, F.J. Hartmann, T. von Egidy, D. Hilscher, W. Bohne, P. Figuera, F. Goldenbaum, U. Jahnke, D. Polster, P. Ziem, J. Galin, B. Lott, M. Morjean, A. Péghaire, B. Quednau, K. Gulda, J. Jastrzebski, W. Kurcewicz, L. Pienkowski, G. Pausch, J. Eades, A.S. Iljinov, M.V. Mebel, Z. Phys. A **359**, 27 (1997).
15. J. Galin, U. Jahnke, J. Phys. G: Nucl. Part. Phys. **20**, 1105 (1994).
16. P. Figuera, W. Bohne, B. Drescher, F. Goldenbaum, D. Hilscher, U. Jahnke, B. Lott, L. Pienkowski, P. Ziem, Z. Phys. A **352**, 315 (1995).
17. F. Goldenbaum, W. Bohne, J. Eades, T. von Egidy, P. Figuera, H. Fuchs, J. Galin, Ye.S. Golubeva, K. Gulda, D. Hilscher, A.S. Iljinov, U. Jahnke, J. Jastrzebski, W. Kurcewicz, B. Lott, M. Morjean, G. Pausch, A. Péghaire, L. Pienkowski, D. Polster, S. Proschitzki, B. Quednau, H. Rossner, S. Schmid, W. Schmid, P. Ziem, Phys. Rev. Lett **77**, 1230 (1996).
18. U. Jahnke, W. Bohne, J. Eades, T. von Egidy, P. Figuera, H. Fuchs, J. Galin, F. Goldenbaum, K. Gulda, Ye.S. Golubeva, F.J. Hartmann, D. Hilscher, A.S. Iljinov, J. Jastrzebski, W. Kurcewicz, B. Lott, M. Morjean, G. Pausch, A. Péghaire, L. Pienkowski, D. Polster, S. Proschitzki, B. Quednau, H. Rossner, S. Schmid, W. Schmid, Phys. Atom. Nucl. **59**, 1567 (1996).
19. B. Lott, W. Bohne, J. Eades, T. von Egidy, P. Figuera, H. Fuchs, J. Galin, F. Goldenbaum, Ye.S. Golubeva, K. Gulda, D. Hilscher, A.S. Iljinov, U. Jahnke, J. Jastrzebski, W. Kurcewicz, M. Morjean, G. Pausch, A. Péghaire, L. Pienkowski, D. Polster, S. Proschitzki, B. Quednau, H. Rossner, S. Schmid, W. Schmid, P. Ziem, Nucl. Phys. B Proc. Suppl. A **56**, 114 (1997).
20. U. Jahnke, W. Bohne, T. von Egidy, P. Figuera, J. Galin, F. Goldenbaum, D. Hilscher, J. Jastrzebski, B. Lott, M. Morjean, G. Pausch, A. Péghaire, L. Pienkowski, D. Polster, S. Proschitzki, B. Quednau, H. Rossner, S. Schmid, W. Schmid, Phys. Rev. Lett. **83**, 4959 (1999).
21. L. Pienkowski, W. Bohne, T. von Egidy, P. Figuera, J. Galin, F. Goldenbaum, D. Hilscher, U. Jahnke, J. Jastrzebski, B. Lott, M. Morjean, G. Pausch, A. Péghaire, D. Polster, S. Proschitzki, B. Quednau, H. Rossner, S. Schmid, W. Schmid, Phys. Lett. B **472**, 15 (2000).
22. R.A. Cecil, B.D. Anderson, R. Madey, Nucl. Instr. Meth. **161**, 439 (1979).
23. D. Hilscher, J.R. Birkelund, A.D. Hoover, W.U. Schröder, W.W. Wilke, J.R. Huizenga, A.C. Mignerey, K.L. Wolf, H.F. Breuer, V.E. Viola, Phys. Rev. C **20**, 576 (1979).
24. F. Goldenbaum, Ph.D. thesis, Freie Universität Berlin 1996, unpublished.
25. D.W. Lang, Nucl. Phys. **53**, 113 (1964).
26. D. Hilscher, U. Jahnke, F. Goldenbaum, L. Pienkowski, J. Galin, B. Lott, Nucl. Instr. Meth. A **414**, 100 (1998).